Radially Distributed Instabilities and Nonlinear Process to Generate Pressure Variation in a Torus Plasma

Naohiro KASUYA and Masatoshi YAGI[1)]

Research Institute for Applied Mechanics, Kyushu University, 6-1 Kasuga-kouen, Kasuga, Fukuoka 816-8580, Japan
[1)]*National Institute for Quantum and Radiological Science and Technology, 2-166 Omotedate, Obuchi, Rokkasho, Aomori 039-3212, Japan*

(Received 14 May 2016 / Accepted 17 January 2017)

Distributed instabilities can successively change one after another to give accelerated radial propagation. The response of the linearly unstable distributed instabilities is identified in a gradual evolution phase as well as in a phase just after impact of modulation. Global nonlinear simulations of drift-interchange modes in helical plasmas are carried out with source modulation using a reduced MHD model. Conditional average of long time-series data with the modulation period reveals characteristic responses of the plasma. Smaller-scale variations comparable to the micro-temporal scale in this simulation are also included in the gradual evolution phase. The correlation analysis shows that the evolution of the mean pressure is strongly correlated with the strength of the nonlinear coupling. The evaluation of the energy balance to decompose the energy transfer into contribution from each three-wave coupling clarifies that a single mode coupling at each location has the dominant contribution to the smaller-scale pressure evolution in spite of self-organized mechanism with a wide range of comparable magnitude modes. Comparison of mode amplitudes does not define the dominant one, so identification of the active mode is useful for understanding the causality. This selection suggests the mechanism that gives the spreading effective in the quasi-steady state as for the ballistic propagation in the self-organized critical state.

Keywords: turbulence spreading, self-organization, global simulation, nonlinear coupling, energy transfer, source modulation, torus plasma

DOI: 10.1585/pfr.12.1303005

It is widely recognized that simple diffusive models are not adequate to describe the transport phenomena in torus plasmas [1]. To capture the nature of the transport, there are several experiments to observe plasma non-diffusive responses [2–4]. In particular, the modulation experiments in the Large Helical Device (LHD) have revealed several unresolved problems, such as a hysteresis in the dependencies of turbulence and transport on the mean pressure gradient [4], and abrupt increase of core temperature associated with edge cooling [5]. A long-range fluctuation with a scale size comparable to the minor radius is observed in the modulation experiment, whose origin is not yet clarified [6]. We have investigated the dynamics of the global pressure profile by use of an extended reduced MHD model in helical plasmas to study the transport mechanisms, and have observed propagation, responding to the core heat modulation [7]. The turbulent spreading is known as the successive response of radially distributed micro-instabilities to give accelerated propagation [8–10]. The successive responses of localized modes to large perturbations have been revealed, however, nonlinear mechanism exists to sustain the self-organized critical level [11, 12]. Therefore, the role of the modes in the saturated state must be clarified, i.e., whether the leading marginally unstable mode at each location can act as a leader by overcoming the extinguishment by the nonlinear sustainment in the saturated state. For that purpose, combination of the turbulence simulation and statistical analysis (conditional averaging [4]) is used. Fluctuations include random evolutions, and conditional averaging is applied to eliminate the randomness and extract the characteristic plasma response. Repetitive modulation of a pressure source term is used as the trigger for the conditional averaging. In this article, a response mechanism of the mean pressure (poloidally and toroidally homogenous component with temporal variation) is investigated by evaluating the energy balance in the nonlinear global simulation. Drift-interchange instability is calculated in a helical plasma, which is localized near the rational surface with $k_\perp a < 100$, where a is the minor radius, and also includes drift wave properties. Mode coupling process similar to drift wave turbulence can be considered in spite of its larger spatial scale. Not only the rapid response to impact of the source change as in [7] but also the whole period of the modulation is analyzed, which reveals that the leading modes plays the role for leading the pressure temporal variation, though there exist several modes that have the same level of nonlinear energy transfer. Note that what we analyze is the response to the modulation, so some typical

author's e-mail: kasuya@riam.kyushu-u.ac.jp

variations remain after the averaging (not everything are smoothed out). The selection of the leading nonlinear coupling with the micro-scale evolution can be an important indicator to describe the variation with sustainment of the self-organized state.

For dynamical simulations, a simulation code has been developed to calculate the electromagnetic nonlinear saturation in toroidal helical plasmas with a circular cross-section [13]. Toroidal coordinate (r, θ, ζ) is used, where the position at $r = 0$ represents the center of the circular cross-section. A set of reduced MHD equations of drift-interchange instability is solved to obtain time evolutions of 3 fields; stream function u, ζ component of the vector potential A and total pressure P. The reduced MHD model to describe the interchange mode in helical plasmas [14] is extended to include a drift wave instability by including the diamagnetic terms in the conduction equation [13]. The model is used as the fundamental one including global and localized modes, nonlinear couplings with the Reynolds stress, and collisional transport processes, and the details are described in [7]. The instabilities can drive heat fluxes to contribute to the pressure variation. The modes are localized at their resonance magnetic surfaces, and the mode width $\sim 0.1a$ is larger than that of typical micro instabilities in torus plasmas, which can be induced with combination to the drift wave mechanism in a helical plasma. The E × B nonlinear couplings between the radially-distributed instabilities have the common feature in torus plasmas, so we use this as the target to investigate the spreading, though there is difference in the spatial scales. Recently turbulence simulations using gyro-kinetic models can show good quantitative agreement to experiments for transport in torus plasmas [15–17], but a global simulation for a long-time series with non-adiabatic electrons, which is necessary for our research, is still difficult due to its large computational costs in helical plasmas [18], so we use the fluid model in this article.

To clarify the dynamical response, source modulation is investigated. Here, the parameter set as same in [7] is used. The magnetic configuration is given by the rotational transform ι in helical plasmas, which is the inverse of the safety factor, as in Fig. 1 (a). With this profile the instability driven by the magnetic curvature distributes as in Fig. 1 (b). This represents the mode amplitudes, and the heat flux driven by them is more localized as shown in Fig. 11 in Ref. [7]. The responses of the modes are investigated with source modulation. For the modulation, the additional source is switched on and off cyclically, which exists mainly near the center of the plasma in the region with $0 < r/a < 0.3$. The modulation cycle is set to be $1000\tau_A$, which is close to the energy confinement time, where $\tau_A = R/V_A$ is the Alfvén time, V_A is the Alfvén velocity, and R is the major radius. There exist large pressure fluctuations, so superposition of source modulation cycles (conditional averaging) is applied to eliminate random fluctuations. The averaging over 40 cycles is carried

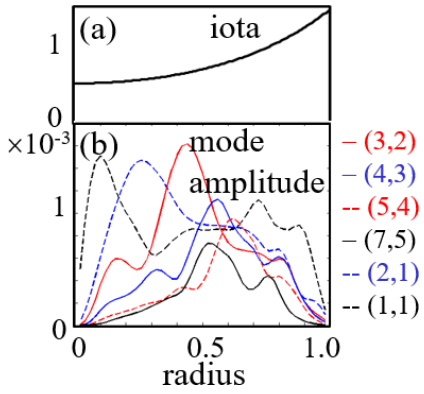

Fig. 1 (a) Rotational transform profile and (b) distribution of the mode amplitudes. Radial profiles of the temporal averaged mode amplitudes are shown in (b).

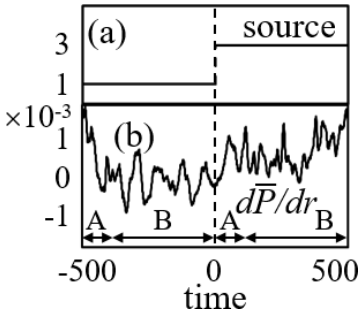

Fig. 2 Response to the modulation. Time evolutions of (a) the applied source amplitude, and (b) the mean pressure gradient at $r/a = 0.6$ are shown. The gradient is obtained by the conditional average with the source modulation period. The periods A and B in panel (b) represent the phase with rapid change just after the source modulation and the gradual evolution phase, respectively.

out in this analysis, which is sufficient for convergence [7]. Figures 2 (a)–(b) show the time evolutions of the pressure source at the center, and the mean pressure gradient at $r/a = 0.6$. At this observation position with $r/a > 0.5$, the direct source change is negligibly small. Both micro-scale (comparable to the transit time by the phase velocity of the mode $50\tau_s \sim 60\tau_A$, where τ_s is the ion acoustic transit time) and meso-scale (several times larger than the former) temporal evolutions can be extracted from the simulation data. Only the variation with the micro-scale is the target in this article.

To clarify the variation mechanism, the balance of the terms in the model equation is decomposed into each contribution. The evolution equation of the internal energy of the (m, n) component is given as

$$\frac{\partial E_{P_{mn}}}{\partial t} = \frac{1}{2C}\int dr^3 P_{mn}{}^* \left\{ \left(-\alpha C \frac{\partial \nabla_\perp{}^2 A}{\partial \zeta} + \alpha C \frac{\partial \Psi_0}{\partial r}\frac{\partial \nabla_\perp{}^2 A}{r\partial\theta} + \eta_\perp \nabla_\perp{}^2 P \right)_{mn} \right.$$
$$\text{TE} \qquad\qquad \text{LN1} \qquad\quad \text{LN2} \qquad \text{LN3}$$
$$\left. + S_{mn} + \left[u, P\right]_{mn} \right\}, \qquad (1)$$
$$\text{ST} \qquad \text{NL}$$

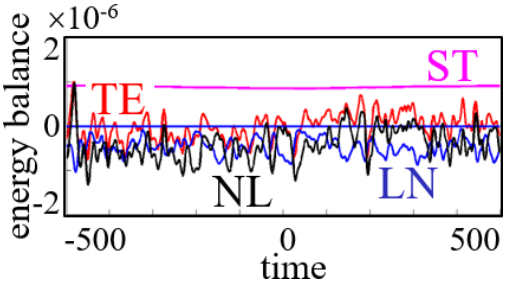

Fig. 3 Time evolution of the energy balance terms in Eq. (1) at $r/a = 0.6$.

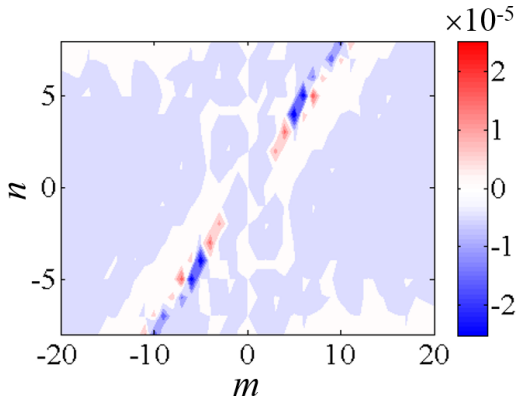

Fig. 4 Nonlinear contribution to the P_{00} component. The averaged contributions NL are decomposed into each (m, n) component at $r/a = 0.6$.

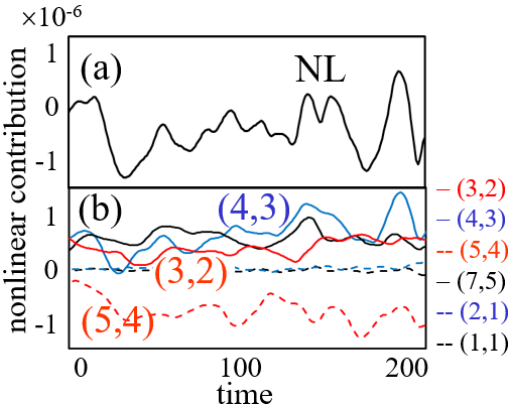

Fig. 5 Time evolution of the nonlinear contribution to the P_{00} component. (a) Total nonlinear contribution at $r/a = 0.6$ and (b) those of prominent modes in Fig. 4 are shown.

where [ ] is the Poisson bracket, S is the source term, m and n are the poloidal and toroidal mode-number, and α, C, Ψ_0, $\eta_\perp$ are defined in [7]. Here, t is normalized by τ_A. The 1st, 2nd and 3rd terms in the right hand side of Eq. (1) come from linear contributions by parallel derivative (LN1, LN2) and diffusion (LN3). The 4th term is from the source (ST), which only contains the $(m, n) = (0, 0)$ component in this case. The 5th term is the nonlinear contribution from convective derivative (NL). We focus on the nonlinearities from the Reynolds stress, and nonlinear terms from the Maxwell stress are not included in the calculations, which is known to have little effect in the low β case [19, 20]. Figure 3 shows the time evolution of the energy balance of the $(m, n) = (0, 0)$ component at $r/a = 0.6$. After the additional source is switched on at $t = 0$, the evolution of the left hand side of Eq. (1) (TE) increases from negative to above zero after a time delay $\sim 40\tau_A$ for propagation of the source increase in the plasma central region [7]. The source contribution (ST) is positive, and LN (summation of LN1-3) and NL are negative for the whole of the duration, so ST is the drive for the pressure profile formation, however the temporal variation of ST is much smaller than that of TE. The correlation coefficient between two time-series data p and q

$$C(p,q) = \frac{\sum_i (p(i) - \bar{p})(q(i) - \bar{q})}{\sqrt{\sum_i (p(i) - \bar{p})^2 \sum_i (q(i) - \bar{q})^2}}, \qquad (2)$$

is used for the evaluation, where $\bar{p}$ represents the temporal average of p. The correlation between TE and NL is larger (correlation coefficient 0.8) than that between TE and LN (correlation coefficient 0.0), so the temporal variation is dictated by the nonlinear contribution from NL, which corresponds to the transport driven by the instabilities to modify the pressure profile. The time evolution indicates that NL and LN are anti-phased with each other, and the correlation analysis shows NL is preceding LN with $\delta t = 3\tau_A$. This is why the pressure variation appears, and the time delay, much smaller than the transit time, corresponds to the duration for adjustment to sustain the saturated level.

The important role of the nonlinear term is confirmed in the evolution, so next the decomposition of mode couplings is carried out to identify the dominant mode affecting the pressure evolution. Figure 4 shows nonlinear contributions NL decomposed into each (m, n) component. In red regions, the P_{00} component gets the energy from modes, and in blue regions, vice versa. The averaged values over $t = 1$–1000 (whole of the cycle) are shown. There is radial distribution of the nonlinear contribution corresponding to the rotational transform profile, and modes with $m/n \sim 1.3$ have large amplitudes at $r/a = 0.6$, where the inverse of the iota is $1/\iota = 1.3$. The modes with $(m, n) = (3, 2), (4, 3), (5, 4), (6, 5), (7, 5), (9, 7), (10, 8), (11, 8)$, etc. are large and have the same order of amplitudes as in Fig. 4. Figure 5 shows the time evolutions of the nonlinear contributions. The total nonlinear contribution in (a) is determined by combination of several mode couplings as in (b). The correlation analysis shows strong correlation with mode $(m, n) = (4, 3)$ (correlation coefficient 0.5), which has the largest amplitude at the position as in Fig. 1 (b), and weak correlation with the other

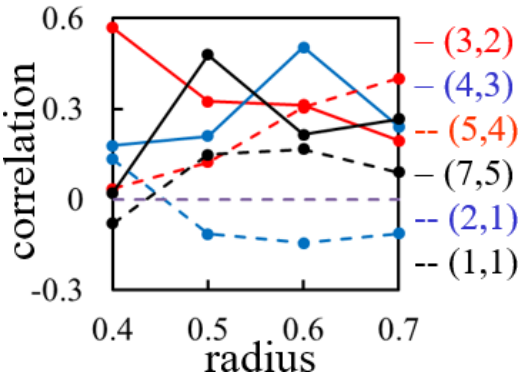

Fig. 6 Radial profiles of the correlations of nonlinear contributions to the P_{00} component. The correlations between the total contribution and those from individual modes are shown.

modes (the second most correlation coefficient is 0.3 with mode $(m, n) = (7, 5)$). The dominant mode couplings for the smaller-scale evolution are different depending on the radial positions, and is not simply the largest amplitude mode at each position. Figure 6 shows the radial profiles of the correlations. There is a single dominant mode at each position, whose resonant position locates nearby. However, at $r/a = 0.5$, for example, the dominant one is mode $(m, n) = (7, 5)$, though the largest amplitude one is mode $(m, n) = (3, 2)$. This is because the mode is possible to be driven passively by nonlinear couplings with the other modes. This is similar to the case of the heat flux; there exists a mode that does not drive the heat flux [7].

In summary, global nonlinear simulations of drift-interchange modes in helical plasmas are carried out to clarify the mechanism of the evolution of mean pressure. Conditional average with the modulation period is used to extract the characteristic response of the plasma, and fluctuations in the phase gradually approaching to the steady state is also analyzed. The evaluation of the energy balance confirms that nonlinear variation is sustained by a wide range of excited modes. It is found that a single linearly unstable mode at each location has the dominant contribution to the smaller-scale pressure evolution. Linearly unstable modes can induce nonlinear modification of the pressure profile by a modulational process, and the profile modification is flattened by the linear diffusion term. There is a time delay of the linear response, so the profile modification appears. The time evolution is led by the dominant mode, so identification of the active mode is useful for understanding the causality in the evolution. The distributed instability has been known to affect the accelerated propagation by the turbulence spreading mechanism, and is found to be effective in a gradual evolution phase as well as in a phase just after a large modulation.

In the simulation there exists another characteristic frequency in the broad band spectrum, which has the longer time-scale than the smaller turbulent time-scale. The oscillation is induced by coupling with the magnetic curvature term, and also appears in the evolution of the mean pressure. It is possible to act as a nonlinear channel for energy redistribution. The oscillation is electromagnetic, which accompanies with variation of the position of a magnetic axis. Change of the magnetic configuration can affect both neoclassical [21] and turbulent [22] transport in the wide region of the plasma, so the effect should be evaluated. For explanation of experimental results of non-local responses, importance of effects in the phase space is pointed out [23]. The model adopted in this article is a simplified one, and inclusion of such effect by applying a gyro-kinetic model is left for future works.

The authors acknowledge discussions with Prof. K. Itoh, Prof. S.-I. Itoh, and Prof. S. Inagaki. This work is supported by JSPS KAKENHI Grant Number JP24760703 and JP16K06938, by the collaboration program of NIFS (NIFS15KNST082, NIFS16KNXN323, NIFS13KOCT001) and of RIAM of Kyushu University. Some numerical simulations were carried out on the Helios Super Computer System at Computational Simulation Center of International Fusion Energy Research Center.

[1] K. Ida *et al.*, Nucl. Fusion **55**, 013022 (2015).
[2] K. Gentle *et al.*, Phys. Rev. Lett. **74**, 3620 (1995).
[3] P. Mantica, P. Galli, G. Gorini, G.M.D. Hogeweij, J. de Kloe, N.J. Lopes Cardozo and RTP Team, Phys. Rev. Lett. **82**, 5048 (1999).
[4] S. Inagaki *et al.*, Nucl. Fusion **53**, 113006 (2013).
[5] N. Tamura *et al.*, Nucl. Fusion **47**, 449 (2007).
[6] S. Inagaki *et al.*, Nucl. Fusion **54**, 114014 (2014).
[7] N. Kasuya, S. Sugita, S. Inagaki, K. Itoh, M. Yagi and S.-I. Itoh, Plasma Phys. Control. Fusion **57**, 044010 (2015).
[8] T.S. Hahm, P.H. Diamond, Z. Lin, K. Itoh and S.-I. Itoh, Plasma Phys. Control. Fusion **46**, A323 (2004).
[9] O.D. Gürcan, P.H. Diamond, T.S. Hahm and Z. Lin, Phys. Plasmas **12**, 032303 (2005).
[10] X. Garbet, Y. Sarazin, F. Imbeaux, P. Ghendrih, C. Bourdelle, O.D. Gürcan and P.H. Diamond, Phys. Plasmas **14**, 122305 (2007).
[11] P.H. Diamond and T.S. Hahm, Plasma Phys. **2**, 3640 (1995).
[12] B.A. Carreras, D. Newman, V.E. Lynch and P.H. Diamond, Phys. Plasmas **3**, 2903 (1996).
[13] N. Kasuya, S. Sugita, M. Sasaki, S. Inagaki, M. Yagi, K. Itoh and S.-I. Itoh, Plasma Fusion Res. **8**, 2403070 (2013).
[14] M. Wakatani, *Stellarator and Heliotron Devices* (Oxford University Press, Oxford, 1998).
[15] X. Garbet, Y. Idomura, L. Villard and T.-H. Watanabe, Nucl. Fusion **50**, 043002 (2010).
[16] M. Nunami, T.-H. Watanabe, H. Sugama and K. Tanaka, Phys. Plasmas **19**, 042504 (2012).
[17] T. Görler, A.E. White, D. Told, F. Jenko, C. Holland and T.L. Rhodes, Phys. Plasmas **21**, 122307 (2014).
[18] P. Helander, T. Bird, F. Jenko, R. Kleiber, G.G. Plunk, J.H.E. Proll, J. Riemann and P. Xanthopoulos, Nucl. Fusion **55**, 053030 (2016).
[19] P.H. Diamond, S.-I. Itoh, K. Itoh and T.S. Hahm, Plasma Phys. Control. Fusion **47**, R35 (2005).
[20] V. Naulin, A. Kendl, O.E. Garcia, A.H. Nielsen and J.J.

Rasmussen, Phys. Plasmas **12**, 052515 (2005).
[21] S. Murakami *et al.*, Nucl. Fusion **42**, L19 (2002).
[22] T.-H. Watanabe, H. Sugama and S. Ferrando-Margalet, Phys. Rev. Lett. **100**, 195002 (2008).
[23] S.-I. Itoh and K. Itoh, Sci. Rep. **2**, 860 (2012).